Geosci. Model Dev. Discuss., doi:10.5194/gmd-2015-251, 2016
Manuscript under review for journal Geosci. Model Dev.
Published: 15 January 2016

Geoscientific Model Development Discussions
Open Access

Spatio-temporal variability in N_2O emissions from a tea-planted soil in subtropical central China

X. L. Liu[1,*], X. Q. Fu[1,*], Y. Li[1], J. L. Shen[1], Y. Wang[1], G. H. Zou[1], Y. Z. Wu[1], Q. M. Ma[1], D. Chen[1], C. Wang[1], R. L. Xiao[1], and J. S. Wu[1]

[1]Changsha Research Station for Agricultural & Environmental Monitoring and the Key Laboratory of Agro-ecological Processes in Subtropical Regions, Institute of Subtropical Agriculture, Chinese Academy of Sciences, Hunan 410125, China
[*]These authors contributed equally to this work.

Received: 16 November 2015 – Accepted: 26 November 2015 – Published: 15 January 2016

Correspondence to: Y. Li (yli@isa.ac.cn)

Published by Copernicus Publications on behalf of the European Geosciences Union.

GMDD
doi:10.5194/gmd-2015-251

Spatio-temporal variability in N_2O emissions

X. L. Liu et al.

Abstract

To explore the intrinsic spatial patterns of N_2O emissions in agricultural systems, not only should the spatial and temporal variability in N_2O emissions be analyzed separately, but the joint spatio-temporal variability should also be explored by applying spatio-temporal semivariogram models and interpolation methods. In this study, we examined the spatio-temporal variability in N_2O emissions from a tea-planted soil from 28 April 2014 to 27 May 2014 using 96 static mini chambers in an approximately regular grid on a 40 m^2 tea field (sampling 30 times), and the results were compared with long-term observations of the N_2O emissions recorded using large static chambers (sampling 5 times). The N_2O fluxes observed by the mini chambers during a 30 min snapshot (10:00–10:30 a.m. China Standard Time) ranged from −2.99 to 487.0 $mg\,N\,m^{-2}\,d^{-1}$ and were positively skewed with a median of 13.6 $mg\,N\,m^{-2}\,d^{-1}$. The N_2O flux data were then log-transformed for normality. After detrending the influences from the chamber placement positions (Position) and the precipitation accumulated over two days (Rain2), the log-transformed N_2O fluxes (FLUX30t) exhibited strong spatial, temporal and joint spatio-temporal autocorrelations, which were used as three components of spatio-temporal semivariogram models and were characterized by models based on Stein's parameterized Matérn (Ste) function, exponential function and again the Ste function, respectively. The spatio-temporal experimental semivariogram of the N_2O fluxes was fitted using four spatio-temporal semivariogram models (separable, product-sum, metric and sum-metric). The sum-metric model performed the best and provided meaningful effective ranges of spatial and temporal dependence, i.e., 0.41 m and 5.4 days, respectively. Four spatio-temporal regression-kriging interpolations were applied to estimate the spatio-temporal distribution of N_2O emissions over the study area. The cross-validation results indicated that the four interpolations exhibited similar performances ($r = 0.817$–0.824, $RMSE = 0.456$–0.486, $p < 0.001$), and outperformed the multiple linear regression prediction ($r = 0.735$, $RMSE = 0.560$, $p < 0.001$). The predictions of the four kriging interpolations for the total N_2O emissions

GMDD
doi:10.5194/gmd-2015-251

from the 40 m^2 tea field ranged from 18.3 to 18.5 g N; these values were approximately 25 % higher than the results predicted using the observations of large static chambers. Furthermore, compared with the other three models, the metric model exhibited weak sensitivity for peak prediction, although the cross-validation results indicated that they had same prediction capabilities. Our findings suggested: (i) that the size of large static chambers used for long-term observations of N_2O fluxes should be no less than 0.4 m and the time interval for gas sampling should be constrained to approximately 5 days; and (ii) that more efficient testing methods should be adopted to replace the conventional cross-validation methods for evaluating the performance of spatio-temporal kriging.

1 Introduction

Each year, 2.8 (1.7–4.8) Tg of nitrous oxide (N_2O) is emitted from agro-ecosystems, significantly contributing to global warming (Ravishankara et al., 2009; IPCC, 2013). Accurate estimates of the amount and characteristics of N_2O emissions are important prerequisites for reducing N_2O emissions from agro-ecosystems (Akiyama et al., 2013; Ambuset al., 1994; Han et al., 2013; Kiese et al., 2003; Konda et al., 2008, 2010; Lin and Han, 2009; Mosier et al., 1996, 1998; Turner et al., 2008). However, N_2O is microbially mediated; it is produced via microbial processes of nitrification under aerobic conditions and denitrification under anaerobic conditions (Firestone and Davidson, 1989; Hayatsu, 1993; Mathieu et al., 2006; Venterea and Rolston, 2000; Wrage et al., 2004; Yanai et al., 2003), and thus, its emissions from soils are strongly affected by certain spatio-temporally variable environmental factors, such as climate, vegetation type, atmospheric deposition, terrain, land management practices, and soil properties (Tokuda and Hayatsu, 2004). Consequently, in agricultural systems, N_2O emissions possess inherent purely spatial, purely temporal and joint spatio-temporal heterogeneities, which have not been sufficiently thoroughly researched because of

GMDD
doi:10.5194/gmd-2015-251

both the inherent complexities of N_2O emissions and our own epistemic defects (Li et al., 2013).

The importance of simultaneously studying the spatial and temporal aspects of N_2O emission processes is well-known (Gorres et al., 1998; Van Kessel et al., 1993; Velthof et al., 1996). To obtain complete information regarding N_2O emissions from soils, classical continuous temporal observations using static box methods and micro meteorological methods (Davidson et al., 1993, 2000), as well as purely spatial-structure-based research (Ball et al., 1997; Clemens et al., 1999; Röver et al., 1999; Folorunso et al., 1984; Li et al., 2013) have been applied in recent decades and have yielded significant results. However, these studies failed to provide a sufficient description of the process of the evolution of N_2O emissions over space and time (Fu et al., 2015). One reason for this failure is that the structural analysis of such spatio-temporal processes is more difficult than that of purely spatial or temporal processes because of the different scales and causality principles that are relevant to the space and time domains (Hengl et al., 2011). In addition to the inherent complexity (ontological factors) of N_2O emissions, e.g., spatio-temporal heterogeneity, our own epistemic defects, which can be primarily attributed to incomplete information, are another important factor that may impact the accuracy of estimates of the total amount of N_2O emissions (Huang et al., 2007).

Traditionally, geostatistical interpolation methods are considered to be state-of-the-art statistical approaches to spatial analysis (Cressie and Wikle, 2011; Kilibarda et al., 2014). The principle goals in geostatistical analysis are to estimate and model the correlations of a spatial process (Goovaerts, 1997; Webster, 1985; Webster and Oliver, 2001). Thus, geostatistics provides several statistical tools to address static spatial variables, including exploring and modeling spatial structures, predicting the unsampled locations and assessing their uncertainties (Webster and Oliver, 2001). In recent years, geostatistical methods for the analysis of spatio-temporal data have garnered considerable interest in many areas of application, but such methods are less well developed than those for the analysis of purely spatial or purely temporal data, partly because of the lack of suitable covariance models, which must satisfy the positive definiteness constraint (Hengl et al., 2012; Ma, 2003a). As mentioned above, a purely spatial interpolation approach, which ignores temporal dependencies, can be regarded as a spatio-temporal interpolation in which all temporal correlations are set to zero (Ma, 2004). Therefore, conversional geostatistics needs to be extended with methods of estimating and quantifying spatio-temporal variations and applying them in spatio-temporal interpolations and stochastic simulations (Heuvelink et al., 2010).

In recent decades, several spatio-temporal semivariogram models have been constructed to address and analyze the spatio-temporal autocorrelation of variables that vary in both time and space (De Iaco et al., 2011, 2013, De Iaco and Posa, 2013; Huang et al., 2007; Kolovos et al., 2004; Ma, 2003a, b, 2004; Xu and Shu, 2014), such as soil water content (Snepvangers et al., 2003), surface water quality (Kolovos et al., 2004), the spread of diseases (Gething et al., 2007), terrestrial daily temperature (Hengl et al., 2012; Kilibarda et al., 2014), soil heavy metals (Yang et al., 2015) and PM_{10} (Gräler et al., 2015). In summary, there are two types of spatio-temporal semivariogram models: separable and non-separable (Hengl et al., 2012). The main difference between them is the different structures of the spatio-temporal covariance functions. In the separable context, several geometrically anisotropic models and several separable covariance structures that yield the product or sum of a purely spatial and a purely temporal covariance have been proposed (Dimitrakopoulos and Lou, 1994). This approach allows efficient estimation and inference, but separable models suffered from unrealistic assumptions and properties, e.g., the spatio-temporal process is considered to be temporally independent (Heuvelink and Griffith, 2010; Sampson and Guttorp, 1992). Therefore, many non-separable spatio-temporal covariance structures that can handle zonal and/or geometric anisotropies and negative covariances have been proposed (Gräler et al., 2015; Heuvelink and Griffith, 2010; Mateu et al., 2008), e.g., the summetric model.

Although many different classes of space–time covariance functions are now available, the selection of an appropriate class of models for a particular variable remains difficult (Fuentes, 2006). In practical modeling, the researcher must face the impor-

GMDD
doi:10.5194/gmd-2015-251

tant decision of which spatio-temporal model is the best for fitting his or her empirical data. In the literatures, there are few published papers that present the comparisons of the performance of various spatio-temporal models (Huang et al., 2007). The selection of an appropriate spatio-temporal model might be achieved based on its geometric features and theoretical properties, i.e., by accounting for the tradeoff among the goodness-of-fit, model complexity and prediction accuracy (Huang et al., 2007). In this study, one of the goals is to compare the spatio-temporal prediction preference among four representative semivariogram models.

The estimation process of kriging for spatio-temporal interpolation does not fundamentally differ, in a mathematical or statistical sense, from those of spatial kriging (Heuvelink et al., 2012). Several geostatistical methods, including simple kriging (SK), ordinary kriging (OK), regression kriging (RK) and cokriging (CK), can be used to predict the N_2O fluxes at the unsampled locations (Goovaerts, 1997; Hengl et al., 2004; Odeh et al., 1995; Webster and Oliver, 2001). In purely spatial interpolation, OK uses theoretical semivariogram models to interpolate the spatial distributions and uncertainty. As more sophisticated kriging technologies, RK and CK methods generally outperform OK and are widely used to predict the spatial distributions of many soil properties (McBratney et al., 2000). Other related auxiliary variables and multiple regressions, such as linear regressions, generalized linear models, generalized added models and regression tree models, are included in the RK and CK methods (Hengl et al., 2004). Compared with CK, spatio-temporal RK has achieved several breakthroughs in spatio-temporal interpolation over the past decade with regard to theoretical concepts and various real-world applications (Hengl et al., 2012).

Many researchers have demonstrated that tea planted soils are important sources of N_2O emissions because of their high levels of N fertilizer application and optimal conditions for N_2O emitting microbe activity (e.g., low soil pH, high temperature and ample moisture). For example, Fu et al. (2010, 2012) found that the annual dynamics of N_2O emissions from a tea field with a nitrogen fertilizer application rate of 450 kg N ha^{-1} yr^{-1} fertilizer application was approximately 17.2 kg N ha^{-1} yr^{-1} in 2010. Hirono and Non-

GMDD
doi:10.5194/gmd-2015-251

aka (2012) found that the total N_2O emissions from a tea field with 520 kg N ha^{-1} yr^{-1} fertilizer applications were 10.6 and 14.8 kg N ha^{-1} yr^{-1} in 2008 and 2009, respectively. Li et al. (2013) and Fu et al. (2015) investigated the spatial structures of N_2O fluxes from tea-planted soils during the dry and wet seasons, respectively, and found that the spatial distributions of the N_2O fluxes were primarily associated with field elevation ($r = -0.42$, $p < 0.001$) in the dry season, and with soil ammonium-N (NH_4N), soil nitrate-N (NO_3N) and soil organic carbon (SOC) ($r = 0.57$–0.71, $p < 0.001$) in the wet season. To the best of our knowledge, no researchers have yet attempted to address and interpolate the daily values of N_2O emissions from tea-planted soils using spatio-temporal regression-kriging at a high resolution. Obviously, investigations of this additional source of information have the potential to improve the mapping and estimation of N_2O emissions.

This study was conducted to further explore the spatio-temporal structures of N_2O emissions from tea-planted soils. The objectives of this study were (i) to evaluate the spatio-temporal variability of N_2O emissions from tea-planted soils in subtropical central China, (ii) to compare the prediction performances among four spatio-temporal variogram models, i.e., the separable, product-sum, metric and sum-metric model; and (iii) to assess the accuracy of the traditional in situ static chamber observation methods by comparison with spatio-temporal regression interpolation.

2 Materials and Methods

2.1 Site description

The field experiment was conducted in a small tea field (40 m^2) in Jinjing, Changsha, in Hunan Province, China (28°32′50″ N, 113°19′58″ E; elevation 100 m) (Fig. 1). The region has a subtropical monsoon climate, with a mean annual air temperature of 17.5 °C and a mean annual precipitation of 1400 mm (from 1979 to 2014). On average, 70 % of the annual precipitation occurs in April, May and June. The daily air temperature

GMDD
doi:10.5194/gmd-2015-251

and precipitation for 2014 were recorded by an automatic weather station (Intelimet A, IMET-ADV2, Dynamax, USA) located next to the studied tea field (Fig. 2). The soil of the field was a Haplic Alisol (FAO/UNESCO soil taxonomy) that was derived from a granitic parental material. Tea (*Camellia sinensis* L., *cv. Baihaozao*) was contour-planted in the catchment 10 years ago using an inter-row spacing of 0.5 m. The N average fertilizer application rates in the tea field was 450 kg N ha^{-1} yr^{-1}, separated into two treatments: one single fertilization treatment of 300 kg N ha^{-1} yr^{-1} with urea during March or April and one treatment of 150 kg N ha^{-1} yr^{-1} with oilseed residues, banded 10–15 cm below the soil surface at the fertilization point (Fu et al., 2012). The SOC, total soil nitrogen and total soil phosphorous contents of the topsoil (0–20 cm) were 11.10, 0.86 and 0.37 g kg^{-1}, respectively.

2.2 Design of the field experiment

2.2.1 Spatio-temporal gas sampling and measurements

In the 40 m^2 tea-planted field, 3 centerlines of tea tree rows were recorded using a locally calibrated differential Geographic Positioning System (DGPS) receiver (Sanding Southern Survey Co., China), and were then used to generate the land use data (at a spatial resolution of 0.1 m, respectively, as shown in Fig. 1c and d). The land use data show the four positions at which the mini chambers were placed, including the inter-row position (8.20 m^2), fertilization point (3.60 m^2), under the tea tree (3.60 m^2) and in the tea tree row (24.6 m^2), as described by Li. et al. (2013). Overall, 96 sampling points were determined, and the Euclidean distances between each point and its nearest neighbors ranged from 0.15 to 0.27 m. The *x*-*y* coordinates and the information about gas sampling positions (inter-row position, fertilization point, under the tea tree and in the tea tree row along the tea row transects) were recorded.

Gas samples were collected at each grid point using a closed mini chamber technique. Each mini chamber set was composed of PVC and had two parts (base and chamber). The base was 0.15 m in diameter and 0.05 m high. The chamber was 0.15 m in diameter and 0.15 m high. For the field operations, the base was gently inserted vertically into the soil two days (26 April 2014) before gas sampling, and the chamber was clipped onto the base, with sponge seals in between to prevent gas leakage, before gas sampling on each day from 28 April to 27 May 2014. Therefore, the effective volume of the static chambers equaled 0.002651 m^3. The gas samples were collected from the headspace between 10:00 and 10:30 a.m. To ensure simultaneous sampling, 4 persons skilled in gas sampling assisted in the field sampling. Each person was responsible for 24 sampling positions (Fig. 1) and began sampling at the same time of 10:00 a.m. At each point, three gas sample replicates were collected from the headspace into pre-evacuated 12 mL vials (Exetainers, Labco, UK) at 0 and 30 min after the chamber body was clipped onto the base. The N_2O concentrations of the gas samples were analyzed using a gas chromatograph (Agilent 7890A, Agilent, USA) that was fitted with a ^{63}Ni-electron capture detector and an automatic sample injector system.

2.2.2 Long-term observations

Beginning on 1 January 2010, four static opaque chambers were set at approximately 10 m intervals near the spatio-temporal sampling points (Fig. 1), to observe the dynamic variations in the N_2O fluxes under conventional tea-field management practice (Fu et al., 2012).

Unlike in the mini chamber technique used for spatio-temporal gas sampling, in each long-term experimental plot, a chamber base collar made of stainless steel that was 0.80 m in width and length and 0.20 m in height was permanently inserted into the soil. The large static chamber was 0.80 m in width and length and had a height of 1.20 m. The gas sampling was carried out between 09:00 and 10:00 a.m. local time at approximately one-week intervals from 1 January 2010 to the present. Each time, to measure the N_2O flux, five gas samples were withdrawn at a interval of 10 min using 60 mL gas-tight plastic syringes after the chamber was inserted into the base collar, which was filled with liquid water as a seal (Chen et al., 2015; Fu et al., 2012). From 28

April 2014 to 27 May 2014, all 5 gas samples collected from the large static chambers on each date were available.

2.3 Data analyses

Descriptive statistical and geostatistical analyses were performed using R (R Development Core Team, 2014) with the spacetime (Pebesma, 2012) and gstat packages (DGUU, 2010). Before the spatio-temporal geostatistical analysis was performed, the spatial and temporal semivariograms were calculated and the theoretical semivariogram models were fit.

2.3.1 N_2O fluxes

The N_2O fluxes (FLUX30, $\mathrm{g\,N\,m^{-2}\,d^{-1}}$) in this study were calculated based on the equation described by Li et al. (2013).

$$\mathrm{FLUX30} = (c_{30} - c_0) \cdot \frac{M_{\mathrm{N_2O}}}{V_0} \cdot \frac{h}{\Delta t} \cdot \frac{T_0}{T_0 + T_{\mathrm{air}}} \cdot \frac{1}{1000} \cdot \frac{2 \cdot M_{\mathrm{N}}}{M_{\mathrm{N_2O}}} \cdot 24 \tag{1}$$

where c_{30} and c_0 are the N_2O concentrations in the mini chamber's headspace at 0 and 30 min, respectively, after the lid of the mini chamber was closed (ppmv); $M_{\mathrm{N_2O}}$ is the molecular weight of N_2O ($\mathrm{g\,mol^{-1}}$); V_0 is the molecular volume ($22.4 \times 10^{-3}\,\mathrm{m^3}$) of N_2O under standard conditions (T_0 = 273 K and pressure = 1013 hPa); M_{N} is the atomic weight of nitrogen ($\mathrm{g\,mol^{-1}}$); h is the chamber height (0.18 m); Δt is the incubation period (0.5 h); T_{air} is the air temperature inside the mini chamber (°C); and 24 represents the conversion factor for converting hours to days.

GMDD
doi:10.5194/gmd-2015-251

Spatio-temporal variability in N_2O emissions

X. L. Liu et al.

2.3.2 Spatio-temporal regression kriging

The N_2O fluxes were assumed to consist of the overall trend and a spatio-temporal residual:

$$z(s,t) = m(s,t) + v(s,t) \quad (2)$$

where s and t are the space–time coordinates; z is the finite set of observed N_2O flux data points; m is the trend representing the deterministic part of the variation, which can be empirically explained using a linear function of auxiliary variables; and v is a zero-mean stochastic residual, which may exhibit spatio-temporal dependencies from which a variogram can be calculated. The residuals at the observation locations can be interpolated via kriging.

In general, the trend m is represented by a function of known covariables over the spatio-temporal domain; for example, elevation, soil ammonium content (NH_4N) and soil nitrate content (NO_3N) have all been used to explain a portion of the variation in the N_2O flux (Fu et al., 2015; Li et al., 2013). The linear trend model is given by the following equation:

$$M(s,t) = \sum_{i=1}^{n} \beta_i f_i(s,t) + \beta_0 \quad (3)$$

where the β_i are the regression coefficients; β_0 is the intercept of the linear model; the $f_i(s,t)$ are the covariables over the spatio-temporal domain, which must be fully known (Heuvelink and Griffith, 2010); and n is the number of covariables.

However, this trend cannot explain all of the variation in the flux, although the covariables are spatially, temporally and spatio-temporally varying (Hengl et al., 2012; Heuvelink and Griffith, 2010). Thus, the residual of $v\ (s,t)$ is assumed to be a second-order stationary spatio-temporal random field. In other words, the variance of v is constant, and the covariance of v at points (s,t) and $(s+h,\ t+u)$ depends only on the distances h and u, where h is the Euclidean spatial distance and u is the temporal interval, e.g., in hours, days or months. The following formulas are the covariance and the variogram, respectively:

$$C_{\mathrm{s,\,t}}(s,h) = \mathrm{Cov}\left[Z(s+h,t+u), Z(s,h)\right] \tag{4}$$

$$\gamma_{\mathrm{s,\,t}}(s,h) = \frac{\mathrm{Var}\left[Z(s+h,t+u) - Z(s,h)\right]}{2} \tag{5}$$

Because the space and time domains are associated with different scales and causality principles, their corresponding procedures for semivariance estimation and variable value prediction are inherently different (Hengl et al., 2012). In practice, several simplifying statistical assumptions and constraints can be introduced to fit the spatio-temporal semivariogram, allowing its coefficients to be estimated and ensuring its positive definiteness (Hengl et al., 2012; Huang et al., 2007). In essence, there are two main types of approaches: separable and non-separable. Separable models are composed of purely spatial and purely temporal semivariogram models, and it is assumed that the spatial and temporal processes are uncorrelated (Huang et al., 2007). Conversely, non-separable models assume that there is a correlation between the spatial and temporal processes, and these models include purely spatial, purely temporal, and/or joint spatio-temporal semivariogram models (Kolovos et al., 2004). In this study, the separable, product-sum, metric and sum-metric models were used to explore the spatio-temporal structures of N_2O fluxes in a tea field. These models are described as follows (Gräler et al., 2015):

Separable model

A separable covariance function is assumed to satisfy:

$$C_{\mathrm{s,\,t}}(h,u) = C_{\mathrm{s}}(h) \cdot C_{\mathrm{t}}(u) \tag{6}$$

Its variogram is given as follows:

$$\gamma_{\mathrm{sep}(h,u)} = \mathrm{sill} \cdot \left[\overline{\gamma}_{\mathrm{s}}(h) + \overline{\gamma}_{\mathrm{t}}(u) - \overline{\gamma}_{\mathrm{s}}(h) \cdot \overline{\gamma}_{\mathrm{t}}(u)\right] \tag{7}$$

GMDD
doi:10.5194/gmd-2015-251

Spatio-temporal variability in N_2O emissions

X. L. Liu et al.

In addition, it is assumed that the sill of the pure spatial and temporal semivariogram is equal to 1. Therefore, 5 parameters (spatial range, spatial partial sill, temporal range, temporal partial range and spatio-temporal sill) must be optimized during the fitting process. The simple structure of the separable model facilitates efficient estimation and inference, but the assumption of separability is highly restrictive and often requires unrealistic assumptions (Hengl et al., 2012; Heuvelink and Griffith, 2010).

Product-sum model

The product-sum covariance is assumed to satisfy:

$$C_{ps}(h,u) = C_s(h) + C_t(u) + k \cdot C_s(h) \cdot C_t(u) \tag{8}$$

$$\gamma_{ps}(h,u) = \left(k \cdot \mathrm{sill}_{\gamma_t(u)} + 1\right) \cdot \gamma_s(h) + \left(k \cdot \mathrm{sill}_{\gamma_s(h)} + 1\right) \gamma_t(u) - k\gamma_s(h) \cdot \gamma_t(u) \tag{9}$$

$$k = \frac{\mathrm{psill}_{\gamma_s(h)} + \mathrm{psill}_{\gamma_t(u)} - \mathrm{sill}_{\gamma_{st}(h,u)}}{\mathrm{psill}_{\gamma_s(h)} \cdot \mathrm{psill}_{\gamma_t(u)}} \tag{10}$$

where $k \geq 0$ ensures the positive definite condition (De Iaco et al., 2011).

Metric model

$$C_m(h,u) = C_{\mathrm{joint}}\left(\sqrt{h^2 + (\kappa \cdot u)^2}\right) \tag{11}$$

$$\gamma_m(h,u) = \gamma_{\mathrm{joint}}\left(\sqrt{h^2 + (\kappa \cdot u)^2}\right) \tag{12}$$

In the metric model, the temporal domain is simply rescaled to match the spatial domain through the application of a spatio-temporal anisotropy correction κ, which projects a three-dimensional geographic space into a two-dimensional spatio-temporal space. Compared with the sum-metric model, the metric model ignores the zonal anisotropies of the experimental variogram.

GMDD
doi:10.5194/gmd-2015-251

Sum-metric model

$$C_{\mathrm{sm}}(h,u) = C_{\mathrm{s}}(h) + C_{\mathrm{t}}(u) + C_{\mathrm{joint}}\left(\sqrt{h^2 + (\kappa \cdot u)^2}\right) \tag{13}$$

$$\gamma_{\mathrm{sm}}(h,u) = \gamma_{\mathrm{s}}(h) + \gamma_{\mathrm{t}}(u) + \gamma_{\mathrm{joint}}\left(\sqrt{h^2 + (\kappa \cdot u)^2}\right) \tag{14}$$

where $C_{\mathrm{sm}}(h,u)$ is the covariance at a distance h in space and a distance u in time; $C_{\mathrm{s}}(h)+C_{\mathrm{t}}(u)$ allows for the presence of zonal anisotropies (different semivariogram sills in different directions); and $C_{\mathrm{joint}}(\sqrt{h^2+(\kappa \cdot u)^2})$ allows for the presence of a geometric anisotropy, represented by the ratio κ. The sum-metric model is treated as a sum of independent stationary spatial, temporal and spatio-temporal components (Heuvelink and Griffith, 2010). The $\gamma_{\mathrm{sm}}(h,u)$ term contain ten parameters, including three sets of nuggets, sills and ranges for the spatial, temporal and spatio-temporal semivariogram models as well as the anisotropy ratio κ.

The four spatio-temporal semivariogram models were fitted by applying the L-BFGS-B parameter optimization algorithm (Gräler et al., 2015). A prerequisite for fitting spatio-temporal models is to find the best overall semivariogram surface. Thus, the parameters and structures of the purely spatial, purely temporal and joint components of the above spatio-temporal covariance and semivariogram models are not necessarily the same (Gräler et al., 2015). These semivariances can be calculated for any spatio-temporal distance (h, u) once these parameters have been estimated from the observed residuals. The four spatio-temporal semivariogram models were used to predict the spatio-temporal distribution of the N_2O emissions from the tea-planted soils investigated in this study. The prediction formula for spatio-temporal kriging is similar to those for spatial kriging as follows:

$$\hat{v} = \boldsymbol{x}(s_0,t_0)\cdot\boldsymbol{\beta} + \boldsymbol{v}'\boldsymbol{V}^{-1}\cdot\left[\overline{\boldsymbol{v}}\left(s_i,t_j\right) - \mathbf{X}\cdot\boldsymbol{\beta}\right] \tag{15}$$

where $\boldsymbol{x}(s_0,t_0)$ is the vector of the predictors at the prediction points; $\boldsymbol{\beta}$ is the vector of regression coefficients estimated using the generalized least-squares method

GMDD
doi:10.5194/gmd-2015-251

(Heuvelink and Griffith, 2010), $\boldsymbol{v}'\boldsymbol{V}^{-1}$ is the vector of weight values for simple kriging, $\overline{\boldsymbol{v}}$ is the vector of the observations $\boldsymbol{v}(s_i, t_j)$, and $\mathbf{X}$ is the design matrix of the predictor variables at the observation points.

The final prediction for variable Z at location (s_i, t_j) is defined as:

$$\hat{z}\left(s_i,t_j\right) = m\left(s_i,t_j\right) + \hat{v} \tag{16}$$

where $m(s_i,t_j)$ is the trend estimated in the multiple linear regression analysis. In this study, the N_2O flux data were log-transformed for normality. It was therefore necessary to back-transform the predictions and the kriging standard deviations of the N_2O fluxes to the original data scale. To satisfying the best linear unbiased estimator principle, trans-Gaussian kriging algorithms adopted from Cressie (1993) were used to back-transform the predicted N_2O fluxes and to compute the kriging standard deviation (Denby et al., 2008; Gräler et al., 2012).

$$Z\left(s_i,t_j\right) = \exp\left[\hat{z}\left(s_i,t_j\right) + \frac{\hat{\sigma}\left(s_i,t_j\right)^2}{2}\right] \tag{17}$$

$$\sigma\left(s_i,t_j\right) = \sqrt{\left\{\exp\left[\hat{\sigma}\left(s_i,t_j\right)^2\right] - 1\right\} \cdot \exp\left[2 \cdot \hat{z}\left(s_i,t_j\right) + \hat{\sigma}\left(s_i,t_j\right)^2\right]} \tag{18}$$

Where $\hat{\sigma}(s_i,t_j)$ is the kriging standard deviation at log-transformed data scale.

2.3.3 Accuracy assessment

The quality of all methods was assessed using statistical measures. For example, the root mean square error (RMSE) and the Pearson's correlation coefficient (r) between the predictions and measurements at known locations were calculated using leaveone-out cross-validation.

$$\mathrm{RMSE} = \sqrt{\frac{1}{n \cdot m} \cdot \sum_{i=1}^{n} \sum_{j=1}^{m} \left[\hat{z}\left(s_i, t_j\right) - z\left(s_i, t_j\right) \right]^2} \tag{19}$$

where $\hat{z}\left(s_i, t_j\right) - z\left(s_i, t_j\right)$ is the difference between the cross-validation prediction and the observed N_2O flux at the space–time point (s_i, t_j), and n is the number of N_2O flux observations ($n = 2880$).

2.3.4 Total amount of N_2O emissions

The total amount of N_2O emissions over the study area ($40\,m^2$) from 28 April to 27 May 2014 was calculated. From the result of the spatio-temporal kriging interpolation, the total amount ($S_{N_2O\_st}$) of N_2O emissions (g N) from 28 April to 27 May 2014 was estimated by the following equation:

$$S_{N_2O\_st} = \sum_{t=1}^{30} \sum_{j=1}^{4000} \mathrm{PRE}_j \cdot a \tag{20}$$

where 4000 is the number of grid cells in the study area; PRE is the value predicted by the spatio-temporal regression-kriging; a is the area of a grid cell ($0.01\,m^2$); 30 is the total number of sampling days; and the subscripts t and j are indices representing days and cells, respectively.

For the large static chamber measurements of the N_2O fluxes, the total predicted amount ($S_{N_2O\_t}$) of N_2O emissions (g N) from 28 April 2014 to 27 May 2015 was estimated using the following equation:

$$S_{N_2O\_t} = \left(\frac{f_1 + f_n}{2} + \sum_{i=1}^{n-1} \frac{(f_{i+1} + f_i) \cdot (\mathrm{DOY}_{i+1} - \mathrm{DOY})}{2} \right) \cdot \frac{30}{\mathrm{DOY}_n - \mathrm{DOY}_1 + 1} \cdot \frac{1}{1000} \cdot A \tag{21}$$

where f is the daily N_2O flux (mg N m^{-2} d^{-1}), the subscript i represents the index of the day corresponding to the discrete daily N_2O flux, DOY denotes the day of the year on the Julian calendar, and A is the total study area (= 40 m^2).

3 Results

3.1 Exploratory data analyses

In the 40 m^2 tea-planted field, the N_2O fluxes observed using the mini chambers in 30 min one-time measurements ($n = 2880$) performed from 28 April to 27 May 2014 ranged from −2.99 to 487 mg N m^{-2} d^{-1}, with a median of 13.6 mg N m^{-2} d^{-1} and a CV of 143 %. The N_2O flux data were positively skewed (Fig. 4a), and their log-transformations were approximately normally distributed (Fig. 4b). As shown in Fig. 3, the N_2O fluxes were the highest at the fertilization points, and the differences in the FLUX30t values among the chamber placement positions were statistically significant ($p < 0.001$). Moreover, the N_2O fluxes at the fertilization and under tea tree points were periodically fluctuating. Compared with the N_2O fluxes observed using the mini chambers, the five N_2O fluxes observed using the large static chambers were approximately equal to the N_2O fluxes in the inter-row and in tea-tree row positions, with relatively low N_2O flux values.

By applying a stepwise multiple linear regression analysis, a prediction model was developed to estimate the log-transformed N_2O fluxes using the following equation (adjusted $R^2 = 0.54$, $n = 2880$, $p < 0.001$; see Table 1):

$$\text{FLUX30t} \sim \text{Position} + \text{Rain2} \tag{22}$$

A categorical variable representing the chamber placement positions (Position) and a continuous variable representing the precipitation accumulated over two days (Rain2) were selected as the predictors, which explained 54 % of the total spatio-temporal vari-

GMDD
doi:10.5194/gmd-2015-251

ability in FLUX30t. Therefore, Position and Rain2 were potential candidates to be used as auxiliary predictors for spatio-temporal regression kriging.

3.2 Spatio-temporal variability in N_2O emissions

Prior to the evaluation of the spatio-temporal variability of the N_2O emissions, the purely spatial and purely temporal variability were each analyzed (Fig. 5a and b). Because the N_2O fluxes were significantly correlated with Position and Rain2, two types of semivariogram models were calculated for the N_2O fluxes. First, FLUX30t was found to exhibit no spatial autocorrelation and a moderate temporal dependency (nug = 0.45; psill = 0.23); these data were characterized by an exponential semivariogram model (Exp) and a theoretical temporal distance parameter of 1.17 days (equivalent to an effective range of 3.51 days). Then, by detrending the influence of Position and Rain2, the spatial and temporal semivariogram sills of the N_2O fluxes both decreased. The N_2O fluxes showed a strong spatial autocorrelation and were characterized by Exp, a theoretical distance parameter of 0.22 (equivalent to an effective range of 0.66) and a zero nugget. The temporal structure was still characterized by an Exp model (psill = 0.14, nug = 0.18) and a theoretical temporal distance parameter of 1.63 (equivalent to an effective range of 4.89). The regression residuals exhibited clear autocorrelations in both space and time. Therefore, spatio-temporal kriging of the residuals was certainly applicable, and these parameters from the purely spatial and temporal semivariograms could be used to derive the parameters of the spatio-temporal semivariogram (Gräler et al., 2015).

Figures 5c and 6 show the sampled (regression residuals) spatio-temporal semivariogram and the four fitted models. Table 2 summarizes the parameter estimates for the four semivariogram models. Note that the spatial semivariogram components were all modeled using Stein's parameterized Matérn (Ste) function, the temporal semivariogram components were all modeled using an exponential function, and the joint components were all modeled using the Ste function. As reflected by its lower RMSE value, the sum-metric model was the best-fitting model. In the sum-metric model, the zero nugget effect in the purely spatial, purely temporal and spatio-temporal components indicated that the model could yield better precision. The three range parameters were different, indicating that the residuals were correlated over distances of approximately 0.41 m on the spatial scale and 5.4 days on the temporal scale; these values could be used as criteria for selecting local neighborhoods in spatio-temporal regression-kriging (Heuvelink and Griffith, 2010; Gräler et al., 2015). Furthermore, the spatio-temporal anisotropy indicated that data at a temporal lag of 1 day exhibited a correlation similar to that of observations that were approximately 0.865 m apart. Apparently, compared with the other semivariogram models, the range (57 m) of the separable model in this study was not rational, indicating that the separable model had no physical significance.

3.3 Performance of the spatio-temporal interpolation of the N_2O emissions

As reflected by the lower RMSE and higher r values in the cross-validation results (Table 3), all of the spatio-temporal kriging interpolations ($r = 0.817$–0.824, RMSE = 0.456–0.486, $p < 0.001$) outperformed the multiple linear regression prediction ($r = 0.735$, RMSE = 0.561, $p < 0.001$). For the four spatio-temporal kriging interpolations, the separable, product-sum, metric and sum-metric semivariogram models exhibited similar performances (Fig. 7).

The spatio-temporal distributions and kriging standard deviation maps of the N_2O emissions interpolated using the four models are presented in the Supplement (Figs. S1–S8). For an in-depth comparison of the spatio-temporal prediction performances of the four models, we recalculated the total amounts of N_2O emissions predicted at the four positions over the 30 days and the amounts for the total study area on each day, respectively. As shown in Table 4, the different models presented different results for the same position, although the cross-validation indicated that they had same prediction capabilities. Compared with the other three models, the metric model exhibited insignificant sensitivity to the peak values (Figs. 8 and 9). Moreover, the amounts of N_2O emissions from tea field from 28 April to 27 May 2014 that were predicted by the four spatio-temporal kriging interpolations were 18.3–18.5 g N; these values were approximately 25 % higher than that estimated based on the large static chamber measurements. According to the results of the high-intensity sampling using the mini chambers and the spatio-temporal regression-kriging analysis with the best performance, the total amount of N_2O emitted from the tea field from 28 April to 27 May 2014 was approximately 18 g N.

4 Discussion

4.1 N_2O fluxes in the tea field

The N_2O emissions from soils exhibit obvious spatio-temporal fluctuations and are significantly higher in rainy conditions (Fu et al., 2012, 2015; Konda et al., 2008). In this study, the median (13.6 $mg\,N\,m^{-2}\,d^{-1}$) and CV (143 %) of N_2O fluxes measured in the tea field were all found to be higher than those in other agricultural systems, such as grasslands (Ambus and Christensen, 1994; Turner et al., 2008),winter wheat (Ball et al., 1997; Clemens et al., 1999; Mathieu et al., 2006), and summer maize (Clemens et al., 1999); the findings were similar to the results for the wet season reported by Fu et al. (2015), predominantly because of the optimal conditions for soil microbe activity (e.g., low soil pH, high temperature and ample moisture) provided by tea planted soils (Li et al., 2013). The observations indicate that tea-planted soils are a source of high emissions, especially in rainy and moist periods (Fu et al., 2015; Li et al., 2013). Moreover, among the four mini chamber positions used in this study, the fertilization points had obviously higher N_2O fluxes values (Fig. 3), indicating that fertilization (300 $kg\,ha^{-1}$, occurred on 19 February 2014) is another important factor of influence on the magnitude of N_2O emissions from tea-planted soils. The primary reason for this effect is that fertilization supplies higher magnitudes of N for soil microbial nitrification and denitrification at the fertilization point, which combined with the optimal conditions for N_2O emissions as mentioned above, results in large amounts of N_2O emissions from tea-planted soils (Fu et al., 2015). The findings are in sharp contrast with the observations

GMDD
doi:10.5194/gmd-2015-251

reported by Li et al. (2013) for the same research area during the dry season, with no fertilization and less rainfall. The reason for this difference may be that the variations in N_2O emissions are impacted by intermittent rainfall (Figs. 2 and 3).

A comparison with the observations from four mini chamber positions reveals that the N_2O fluxes sampled using the large static chambers were obviously lower than those sampled by the mini chamber positions at the fertilization points and did not exhibit fluctuations (Fig. 3). These differences can be primarily attributed to the large size of the static chambers, which covered all four positions and monitored their mean values. Moreover, the mini chambers captured the temporal variations in the N_2O fluxes, whereas the large chambers reflected a trend that was stationary in time. One reason was that the one week interval between gas sampling instances unintentionally avoided the N_2O emission peak, which can strongly influence the accuracy of regional N_2O emissions estimates (Akiyama et al., 2013; Ambus and Christensen et al., 1994; Kiese et al., 2003; Mosier et al., 1996, 1998). Thus, a suitable temporal interval for gas sampling should be determined based on an analysis of the spatio-temporal structure of the N_2O emissions from the tea-planted field.

4.2 Spatio-temporal structure of the N_2O emissions from the tea field

The complex spatio-temporal structural characteristics of N_2O emissions from tea-planted soils can be attributed to influences from factors that also exhibit spatial or spatio-temporal heterogeneity, such as soil types, topography, land management strategies and climate (Firestone and Davidson, 1989; Fu et al., 2015; Hayatsu, 1993; Li et al., 2013; Mathieu et al., 2006; Venterea and Rolston, 2000; Wrage et al., 2004). In this study, three types of structures were analyzed: purely spatial, purely temporal and spatio-temporal. The structures of the N_2O emissions from the tea-planted soils differed significantly between the purely spatial and purely temporal scales. The primary reason for this difference was that the land management procedures, e.g., fertilization, directly impacted the spatial structure and the climate, e.g., rainfall and temperature, directly impacted the temporal structure. No spatial dependence was observed in the spatial structure of the N_2O emissions from the tea field in contrast to the results reported by Li et al. (2013) and Fu et al. (2015). This discrepancy can be primarily attributed to the gas sampling scales, i.e., 40 m^2 in this study and 40 000 m^2 in the previous two studies. Moreover, in this study, although the disturbance of tea-planted soil was very low, the strong influences of fertilization and precipitation still affected the spatial structure of the N_2O emissions on a small scale (Fig. 5).

For a more in-depth analysis of the primary factors influencing the spatio-temporal structures of the N_2O emissions from the tea planted field, we detrended the data with regard to the influence of environmental factors (Position and Rain2) when calculating the spatial, temporal and spatio-temporal semivariograms of the N_2O fluxes. Because the influence of the chamber position on the spatial structure was more relevant than the influence of rain2 on temporal structure, detrending with respect to the influences of Position and Rain2 had more obvious effect on the spatial structure than on the temporal structure (Fig. 5). The effective range of spatial dependence was approximately 0.4 m; this finding could be used as a scientific basis for the design of monitoring scheme using large static chambers in tea-planted fields. Furthermore, the effective range of temporal dependence (5.3 days) could be used to define the time interval for gas sampling in tea-planted fields. Generally, the gas sampling interval for long-term observations of N_2O emissions using large static chambers was one week (Chen et al., 2015; Fu et al., 2012), which may miss several key peaks in N_2O emissions as well as in this study (Fig. 3).

Unlike in previous studies of the purely spatial structure of N_2O emissions from tea-planted soils (Li et al., 2013; Fu et al., 2015), in this study, no soil samples were collected from the soils inside the mini chambers during the sampling period. Therefore, the soil properties, e.g., NH_4N, NO_3N, soil volumetric water content (SWC), could not be directly considered to determine the key environmental factors controlling N_2O emissions or to improve the prediction accuracy of the kriging interpolations. However, the N_2O fluxes were found to be significantly related to Position and Rain2, which reflected the influences of fertilization (NH_4N and NO_3N) and the soil moisture status (SWC), respectively. Our findings were similar to those of Fu et al. (2015) for a fertilized tea field during the wet season. As in other agricultural soils (Ball et al., 1997; Mathieu et al., 2006; Yanai et al., 2003), fertilization contributes to the spatial pattern of the N_2O fluxes from the tea-planted fields, with the highest average fluxes being observed at the fertilization points (Fu et al., 2015). With regard to rainfall, it is possible that rainfall affects the soil moisture and then regulates the variations in the availability of oxygen in tea planted soils, thereby causing spatio-temporal heterogeneity in N_2O emissions by inducing different degrees of soil nitrification and denitrification (Firestone and Davidson, 1989; Fu et al., 2015; Konda et al., 2010).

In this study, considering the tradeoff between the goodness-of-fit and the model complexity, four spatio-temporal semivariogram models were used to fit experimental semivariograms to determine which approach could yield the most appropriate spatio-temporal semivariogram and most accurately predict the spatio-temporal N_2O emissions. The performances of the models differed significantly because of the different model assumptions and properties (De Iaco et al., 2011; Huang et al., 2007). For example, the sum-metric model, which was the best-performing model in this study, fits both zonal anisotropies and the geometric anisotropy (Hengl et al., 2012), whereas the metric model considers only the geometric anisotropy and is unable to fit different semivariogram sills in different directions. The same limitation is also present in the separable model (Ma, 2003a, b and 2004).

4.3 Spatio-temporal interpolation of N_2O emissions

In accordance with the different fitting performances of the four spatio-temporal semivariogram models, four regression-kriging interpolations were applied to predict the spatio-temporal distributions of the N_2O emissions from the tea-planted soils. All four regression-kriging interpolations outperformed the multiple linear regression, indicating that spatio-temporal regression-kriging is an appropriate method for studying the spatio-temporal variations in N_2O emissions from tea-planted soils. Nevertheless, in contrast to the obvious differences among the fits of the semivariogram models, the cross-validation results for the regression-kriging interpolations were not significantly different (Table 4). A similar discrepancy was also observed by Gräler et al. (2015) and can be predominantly attributed to two factors. First, cross-validation methods may be not applicable to spatio-temporal kriging studies. Compared with purely spatial kriging, spatio-temporal kriging encounters more difficulty and uncertainty in predicting the values for unsampled locations, which amplifies the deficiency of cross-validation methods that they are ineffective at reflecting information that is not directly present in the data (Webster, 1985; Webster and Oliver, 2001). Second, the discrepancy between the fit performance and the interpolation performance as evaluated via cross-validation may be due to the inherent complexities of the N_2O emission process, e.g., nitrification and denitrification (Mathieu et al., 2006; Venterea and Rolston, 2000; Wrage et al., 2004; Yanai et al., 2003), and problems of causality in the temporal domain, e.g., the use of values from the future to explain and estimate the past being conceptually awkward and leading to artifacts (Hengl et al., 2012; Huang et al., 2007; Snepvangers et al., 2003).

Although the cross-validation results for the four spatio-temporal regression-kriging interpolations were superficially similar, there were obvious differences among the spatio-temporal distributions and total amounts of N_2O emissions from the tea-planted soils that were predicted by the four spatio-temporal regression-kriging interpolations (Figs. S1–S4). These differences can be directly attributed to the weight values estimated using the semivariogram models during the kriging prediction process (Huang et al., 2007). The different structures of the spatio-temporal semivariogram models were the inherent reason for these differences (Gräler et al., 2015). As mentioned above, both zonal anisotropies and geometric anisotropy play important roles in spatio-temporal structure analysis (Hengl et al., 2012). Zonal anisotropies arise when the amount of variation on temporal scale is smaller or greater than that on spatial scale or the joint spatio-temporal scale (Heuvelink et al., 2010). In this study, the separable, product-sum and sum-metric models all included a zonal anisotropy component, i.e., the sum component of the semivariogram model function, whereas the metric model included only a geometric anisotropy component for the prediction of unsampled points. This fact could also explain why the metric model, which yielded a relatively poor fit, demonstrated better performance in the cross-validation and a lower sensitivity for predicting peak values (Table 4; Fig. 9). In summary, the separable and metric models suffer from unrealistic assumptions and properties and poor spatio-temporal prediction performance, respectively (Hengl et al., 2012; this study). Thus, the product-sum and sum-metric models are considered to be better choices for studying spatio-temporal structure of N_2O emissions.

The total amount of N_2O emissions predicted based on the data from the mini chambers was 25 % greater than that observed by the large chambers. This phenomenon can be primarily attributed to the gas sampling interval (7 days) used for the large static chambers, which could not completely capture the temporal pattern of the N_2O emissions. In particular, two peaks in the N_2O emissions, on 4 and 11 May, were missed (Fig. 3). This observation is also consistent with the effective range of the temporal variability reported above (5.3 days) based on the spatio-temporal structure analysis. However, even if the gas sampling interval for the large static chambers is reduced to 5 days, the strong spatial variability in the N_2O emissions from tea-planted soils will be another important factor giving rise to differences between the results recorded using mini and large static chambers. One may argue that the 25 % differences between the two methods should be due to the differences in barometric pressure between the mini and large static chambers. To address this possibility, several experiments were performed, which demonstrated that any such influence was very subtle and could not be monitored. In summary, both the gas sampling interval and the effects of spatial variability contributed to the difference in the values obtained using the two methods. Thus, in future studies, the gas sampling frequency for large static chambers should be increased and the stainless steel sampling bases should be moved to positions that are several meters away from their previous positions.

GMDD
doi:10.5194/gmd-2015-251

5 Conclusions

During a 30 day in situ field investigation (28 April to 27 May 2014), once-daily 30 min measurements of N_2O emissions from a 40 m^2 red-soil tea field in the subtropical region of central China were recorded at 96 points, and the results were compared with long-term observations of the N_2O emissions recorded using large static chambers. The N_2O fluxes exhibited obvious spatio-temporal differences. Four spatio-temporal semivariogram models, i.e., the separable, product-sum, metric and sum-metric models, were used to fit experimental semivariograms of the N_2O fluxes, and to predict the spatio-temporal N_2O flux distribution using spatio-temporal regression-kriging. The sum-metric model performed best and yielded meaningful effective ranges of the spatial and temporal autocorrelations. The four spatio-temporal regression-kriging interpolations outperformed predictions based on multiple linear regression prediction. The predictions of the four kriging interpolations regarding the total N_2O emissions of the 40 m^2 tea field were approximately 25 % higher that the result observed using the large static chambers.

More spatio-temporal semivariogram models should be created to properly fit the complex surface of the three-dimensional structures of the spatio-temporal variables. More efficient testing methods should be adopted to replace the conventional cross-validation methods because such methods are incapable of evaluating the performance of different spatio-temporal semivariogram models in spatio-temporal kriging. Long-term observations of N_2O emissions should be recorded in a higher density sampling experiment, in which the spatial and temporal sampling intervals should be adjusted to improve the accuracy of the N_2O flux estimates and avoid wasting resources. Moreover, various ecological management treatments, such as intercropping green manure, deep fertilization and the combined application of organic manure and chemical fertilizer, must be applied to reduce N_2O emissions.

GMDD
doi:10.5194/gmd-2015-251
Spatio-temporal variability in N_2O emissions
X. L. Liu et al.

Author contributions. Y. Li designed the experiments and X. Q. Fu, X. L. Liu, J. L. Shen, Y. Wang, G. H. Zou, Q. M. Ma, D. Chen and C. Wang carried them out. X.L. Liu prepared the manuscript with contributions from all co-authors.

Acknowledgements. The National Basic Research Program of China (2012CB417105) and the National Natural Science Foundation of China (41171200 and 41301202) financially supported this research.

References

Akiyama, H., Yan, X. Y., and Yagi, K.: Estimations of emission factors for fertilizer-induced direct N_2O emissions from agricultural soils in Japan: summary of available data, Soil Sci. Plant Nutr., 52, 774–787, 2006.

Ambus, P. and Christensen, S.: Measurement of N_2O emission from a fertilized grassland: an analysis of spatial variability, J. Geophys. Res., 99, 16557–16567, 1994.

Ball, B. C., Horgan, G. W., Clayton, H., and Parker, J. P.: Spatial variability of nitrous oxide fluxes and controlling soil and topographic properties, J. Environ. Qual., 26, 1399–1409, 1997.

Chen, D., Fu, X. Q., Wang, C., Liu, X. L., Li, H., Shen, J. L., Wang, Y., Li, Y., and Wu, J. S.: Nitrous oxide emissions from a Masson pine forest soil in subtropical central China, Pedosphere, 25, 263–274, 2015.

Clemens, J. Schillinger, M. P., Goldbach, H., and Huwe, B.: Spatial variability of N_2O emissions and soil parameters of an arable silt loam – a field study, Bio. Fert. Soils, 28, 403–406, 1999.

Cressie, N.: Statistics for Spatial Data, Wiley, New York, 1993.

Cressie, N. and Wikle, C.: Statistics for Spatio-Temporal Data, Wiley, NJ, 2011.

Davidson, E. A., Matson, P. A., Vitousek, P. M., Riley, R., Dunkin, K., García-Méndez, G., and Maass, J. M.: Processes regulating soil emissions of NO and N_2O in a seasonally dry tropical forest, Ecology, 74, 130–139, 1993.

Davidson, E. A., Keller, M., Erickson, H. E., Verchot, L. V., and Veldkamp, E.: Testing a conceptual model of soil emissions of nitrous and nitric oxides, Bioscience, 50, 667–680, 2000.

De Iaco, S., Myers, D. E., and Posa, D.: On strict positive definiteness of product and product–sum covariance models, J. Stat. Plan. Infer., 141, 1132–1140, 2011.

De Iaco, S. and Posa, D.: Positive and negative non-separability for space–time covariance models, J. Stat. Plan. Infer., 143, 378–391, 2013.

De Iaco, S., Posa, D., and Myers, D. E.: Characteristics of some classes of space–time covariance functions, J. Stat. Plan. Infer., 143, 2002–2015, 2013.
Denby, B., Schaap, M., Segers, A., Builtjes, P., and Horlek, J.: Comparison of two data assimilation methods for assessing PM_{10} exceedances on the European scale, Atmos. Environ., 42, 7122–7134, 2008.
Dimitrakopoulos, R. and Luo, X.: Spatiotemporal Modeling: Covariances and Ordinary Kriging Systems, Geostatistics for the Next Century, Kluwer Academic Publishers, Springer Netherlands, 1994.
DGUU (Department of Geography, Utrecht University): Introduction for Gstat, available at: http://www.gstat.org/index.html (last access: 15 December 2010), 2010.
Firestone, M. and Davidson, E.: Microbial basis of NO and N_2O production and consumption, in: Exchange of Trace Gases Between Ecosystems and the Atmosphere, edited by: Andreae, M. O., and Schimel, D. S., John Wiley, Chichester, 7–21, 1989.
Folorunso, O. A. and Rolston, D. E.: Spatial variability of field measured denitrification gas fluxes, Soil Sci. Soc. Am. J., 48, 1214–1219, 1984.
Fu, X. Q., Li, Y., Xiao, R. L., Tong, C. L., and Wu, J. S.: N_2O emissions from a tea field in subtropical China, in: Proceedings of the 19th World Congress of Soil Science, Soil Solutions for a Changing World, 1–6 August 2010, Brisbane (published on CDROM), 161–163, 2010.
Fu, X. Q., Li, Y., Su, W. J., Shen, J. L., Xiao, R. L., Tong, C. L., and Wu, J. S.: Annual dynamics of N_2O emissions from a tea field in southern subtropical China, Plant Soil Environ., 58, 373–378, 2012.
Fu, X., Liu, X., Li, Y., Shen, J., Wang, Y., Zou, G., Li, H., Song, L., and Wu, J.: Wet-season spatial variability in N_2O emissions from a tea field in subtropical central China, Biogeosciences, 12, 3899–3911, doi:10.5194/bg-12-3899-2015, 2015.
Fuentes, M.: Testing for separability of spatial–temporal covariance functions, J. Stat. Plan. Infer., 136, 447–466, 2006.
Gething, P., Atkinson, P., Noor, A., Gikandi, P., Hay, S., and Nixon, M.: A local space–time kriging approach applied to a national outpatient malaria dataset, Comput. Geosci., 33, 1337–1350, 2007.
Goovaerts, P.: Geostatistics for Natural Resources Evaluation, Oxford University Press, New York, 483 pp., 1997.
Görres, J. H., Dichiaro, M. J., Lyons, J. B., and Amador, J. A.: Spatial and temporal patterns of soil biological activity in a forest and an old field, Soil Biol. Biochem., 30, 219–230, 1998.

GMDD
doi:10.5194/gmd-2015-251

Spatio-temporal variability in N_2O emissions

X. L. Liu et al.

Gräler, B., Rehr, M., Gerharz, L., and Pebesma, E.: Spatio-temporal analysis and interpolation of PM_{10} measurements in Europe for 2009, ETC/ACM Technical paper 2012/8, March 2013.
Gräler, B., Pebesma, E., and Heuvelink, G.: Spatio-temporal interpolation using gstat, available at: https://cran.r-project.org/web/packages/gstat/vignettes/spatio-temporal-kriging.pdf, last access: 5 June 2015.
Han, W., Xu, J., Wei, K., Shi, W., and Ma, L.: Estimation of N_2O emission from tea garden soils, their adjacent vegetable garden and forest soils in eastern China, Environ. Earth Sci., 70, 2495–2500, 2013.
Hayatsu, M.: The lowest limit of pH for nitrification in tea soil and isolation of an acidophilic ammonia oxidizing bacterium, Soil. Sci. Plant Nutr., 39, 219–226, 1993.
Hengl, T., Heuvelink, G. B. M., Perčec Tadić, M., and Pebesma, E. J.: Spatio-temporal prediction of daily temperatures using time-series of MODIS LST images, Theor. Appl. Climatol., 107, 265–277, 2012.
Hengl, T., Heuvelink, G. B. M., and Stein, A.: A generic framework for spatial prediction of soil variables based on regression-kriging, Geoderma, 120, 75–93, 2004.
Heuvelink, G. B. M. and Griffith, D. A.: Space–time geostatistics for geography: a case study of radiation monitoring across parts of Germany, Geog. Anal., 42, 161–179, 2010.
Hirono, Y. and Nonaka, K.: Nitrous oxide emissions from green tea fields in Japan: contribution of emissions from soil between rows and soil under the canopy of tea plants, Soil. Sci. Plant Nutr., 58, 384–392, 2012.
Huang, H. C., Martinez, F., Mateu, J., and Montes, F.: Model comparison and selection for stationary space–time models, Comput. Stat. Data Anal., 51, 4577–4596, 2007.
IPCC: Climate change 2013: the physical science basis. Contribution of working group I, in: Fourth assessment report of the intergovernmental panel on climate change, edited by: Solomon, S., Qin, D., Manning, M., Chen, Z., Marquis, M., Averyt, K. B., Tignor, M., and Miller, H. L., Cambridge University Press, Cambridge, 996 pp., 2013.
Kiese, R., Hewett, B., Graham, A., and Butterbach-Bahl, K.: Seasonal variability of N_2O emissions and CH_4 uptake by tropical rainforest soils of Queensland, Australia, Global Biogeochem. Cy., 17, 1043, doi:10.1029/2002GB002014, 2003.
Kilibarda, M., Hengl, T., Heuvelink, G. B. M., Gräler, B., Pebesma, E., Perčec Tadić, M., and Bajat, B.: Spatio-temporal interpolation of daily temperatures for global land areas at 1 km resolution, J. Geophys. Res., 119, 2294–2313, 2014.

Kolovos, A., Christakos, G., Hristopulos, D. T., and Serre, M. L.: Methods for generating non-separable spatiotemporal covariance models with potential environmental applications, Adv. Water Resour., 27, 815–830, 2004.

Konda, R., Ohta, S., Ishizuka, S., Arai, S., Ansori, S., Tanaka, N., and Hardjono, A.: Spatial structures of N_2O, CO_2, and CH_4 fluxes from Acacia mangium plantation soils during a relatively dry season in Indonesia, Soil Biol. Biochem., 40, 3021–3030, 2008.

Konda, R., Ohta, S., Ishizuka, S., Heriyanto, J., and Wicaksono, A.: Seasonal changes in the spatial structures of N_2O, CO_2 and CH_4 fluxes from Acacia mangium plantation soils in Indonesia, Soil Biol. Biochem., 42, 1512–1522, 2010.

Li, Y., Fu, X., Liu, X., Shen, J., Luo, Q., Xiao, R., Li, Y., Tong, C., and Wu, J.: Spatial variability and distribution of N_2O emissions from a tea field during the dry season in subtropical central China, Geoderma, 193, 1–12, 2013.

Lin, Y. and Han, W.: N_2O emissions from different soils, Chin. J. Tea Sci., 29, 456–464, 2009.

Ma, C.: Families of spatio-temporal stationary covariance models, J. Stat. Plan. Infer., 116, 489–501, 2003a.

Ma, C.: Spatio-temporal stationary covariance models, J. Multivariate Anal., 86, 97–107, 2003b.

Ma, C.: Spatial autoregression and related spatio-temporal models, J. Multivariate Anal., 88, 152–162, 2004.

Mathieu, O., Lévêque, J., Hénault, C., Milloux, M. J., Bizouard, F., and Andreux, F.: Emissions and spatial variability of N_2O, N_2 and nitrous oxide mole fraction at the field scale, revealed with ^{15}N isotopic techniques, Soil Biol. Biochem., 38, 941–951, 2006.

McBratney, A. B., Odeh, I. O. A., Bishop, T. F. A., Dunbar, M. S., and Shatar, T. M.: An over-view of pedometric techniques for use in soil survey, Geoderma, 97, 293–327, 2000.

Mosier, A. R., Duxbury, J. M., Freney, J. R., Heinemeyer, O., and Minami, K.: Nitrous oxide emissions from agricultural fields: assessment, measurement and mitigation, Plant Soil, 181, 95–108, 1996.

Mosier, A. R., Kroeze, C., Nevison, C., Oenema, O., Seitzinger, S., and van Cleamput, O.: Closing the global N_2O budget: nitrous oxide emissions through the agricultural nitrogen cycle, Nutr. Cycl. Agroecosys., 52, 225–248, 1998.

Odeh, I. O. A., McBratney, A. B., and Chittleborough, D. J.: Further results on prediction of soil properties from terrain attributes: heterotopic cokriging and regression kriging, Geoderma, 67, 215–226, 1995.

Pebesma, E.: Spacetime: spatio-temporal data in R, J. Stat. Software, 51, 1–30, 2012.
R Development Core Team: R: a language and environment for statistical computing. R Foundation for Statistical Computing, Vienna, Austria, available at: http://www.R-project.org/, last access: 5 June 2014.
Ravishankara, A. R., Daniel, J. S., and Portmann, R. W.: Nitrous oxide (N_2O): the dominant ozone-depleting substance emitted in the 21st century, Science, 326, 123–125, 2009.
Röver, M., Heinemeyer, O., Munch, J. C., and Kaiser, E. A.: Spatial heterogeneity within the plough layer: high variability of N_2O emission rates, Soil Biol. Biochem., 31, 167–173, 1999.
Snepvangers, J. J. J. C., Heuvelink, G. B. M., and Huisman, J. A.: Soil water content interpolation using spatio-temporal kriging with external drift, Geoderma, 112, 253–271, 2003.
Tokuda, S. I. and Hayatsu, M.: Nitrous oxide flux from a large amount of nitrogen fertilizer and soil environmental factors controlling the flux, Soil. Sci. Plant Nutr., 50, 365–374, 2004.
Turner, D. A., Chen, D., Gellbally, I. E., Li, Y., Edis, R. B., Leuning, R., Kelly, K., and Phillips, F.: Spatial variability of nitrous oxide emissions from an Australian irrigated dairy pasture, Plant Soil, 309, 77–88, 2008.
Van Kessel, C., Pennock, D. J., and Farrell, R. E.: Seasonal-variations in denitrification and nitrous oxide evolution at the landscape scale, Soil Sci. Soc. Am. J., 57, 988–995, 1993.
Velthof, G. L., Jarvis, S. C., Stein, A., Allen, A. G., and Oenema, O.: Spatial variability of nitrous oxide fluxes in mown and grazed grasslands on a poorly drained clay soil, Soil Biol. Biochem., 28, 1215–1225, 1996.
Venterea, R. T. and Rolston, D. E.: Mechanisms and kinetics of nitric and nitrous oxide production during nitrification in agricultural soil, Glob. Change Biol., 6, 303–316, 2000.
Webster, R.: Quantitative spatial analysis of soil in the field, in: Advances in Soil Science, edited by: Stewart, B. A., Springer, New York, 1–70, 1985.
Webster, R. and Oliver, M. A.: Geostatistics for Environmental Scientists, John Wiley & Sons, Chichester, 2001.
Wrage, N., Velthof, G. L., Laanbroek, H. J., and Oenema, O.: Nitrous oxide production in grassland soils: assessing the contribution of nitrifier denitrification, Soil Biol. Biochem., 36, 229–236, 2004.
Xu, J. and Shu, H.: Spatio-temporal kriging based on the product-sum model: some computational aspects, Earth Sci. Inform., 8, 639–648, 2015.
Yanai, J., Sawamoto, T., Oe, T., Kusa, K., Yamakawa, K., Sakamoto, K., Naganawa, T., Inubushi, K., Hatano, R., and Kosaki, T.: Atmospheric pollutants and trace gases: spatial vari-

ability of nitrous oxide emissions and their soil-related determining factors in an agricultural field, J. Environ. Qual., 32, 1965–1977, 2003.
Yang, Y., Wu, J., and Christakos, G.: Prediction of soil heavy metal distribution using Spatiotemporal Kriging with trend model, Ecol. Indic., 56, 125–133, 2015.

GMDD
doi:10.5194/gmd-2015-251

Table 1. Coefficients and standard errors of the multiple linear regressions model for predicting the log-transformed N_2O fluxes ($n = 2880$).

Predictor	Coefficient	Standard error	t value	P value
Intercept	5.95	2.24×10^{-2}	267	$< 0.001^*$
Position2	1.45	2.95×10^{-2}	49.5	$< 0.001^*$
Position3	0.738	2.95×10^{-2}	25.2	$< 0.001^*$
Position4	0.293	2.95×10^{-2}	9.91	$< 0.001^*$
Rain2	8.09×10^{-3}	0	19.4	$< 0.001^*$

* Significant at $P < 0.001$. Rain2 = cumulative precipitation over 2 d before sampling; POSITION2 = fertilization point; POSITION3 = under the tea tree; POSITION4 = in the tea tree row.

GMDD
doi:10.5194/gmd-2015-251

Title Page
Abstract | Introduction
Conclusions | References
Tables | Figures
◀| |▶
◀ ▶
Back | Close
Full Screen / Esc
Printer-friendly Version
Interactive Discussion

Table 2. Parameters of the fitted separable, product-sum, sum-metric and metric models for the N_2O flux regression residuals.

Model	Fitting RMSE	Nugget_s	Sill_s	Range_s (m)	Nugget_t	Sill_t	Range_t (days)	Nugget_{st}	Sill_{st}	Range_{st}	Anisotropy ratio (m d^{-1})
Separable	1.16×10^{-2}	0.236	–	56.8	0.257	–	10.4	–	0.430	–	–
Product-sum	7.71×10^{-3}	0	0.159	0.276	0	0.178	1.72	0	0.284	–	–
Metric	3.65×10^{-2}	7.93×10^{-3}	0.421	3.57	–	–	–	–	–	–	0.345
Sum-metric	6.68×10^{-3}	0	0.112	0.186	0	9.39×10^{-2}	1.72	0	0.137	1.56	0.865

GMDD
doi:10.5194/gmd-2015-251

Table 3. Accuracy assessment parameters for the spatio-temporal regression kriging models. r_{rr} and $r_{FLUX30t}$ denote the Pearson's correlation coefficients between observations and cross-validation predictions of the N_2O flux regression residuals (rr) and the log-transformed N_2O fluxes (FLUX30t), respectively. The N_2O flux regression residuals obtained from the multiple linear regression with the chamber placement positions (Position) and precipitation accumulated over two days (Rain2) as the predictors.

Model	me (dimensionless)	RMSE (dimensionless)	r_{rr}	$r_{FLUX30t}$
Separable	8.23×10^{-4}	0.456	0.563	0.821
Product-sum	8.14×10^{-4}	0.456	0.566	0.822
Metric	5.44×10^{-3}	0.486	0.564	0.824
Sum-metric	5.82×10^{-4}	0.461	0.558	0.817

GMDD
doi:10.5194/gmd-2015-251

Table 4. Total amounts (*g*) of N_2O emissions from the tea-planted soil at the four positions predicted by the spatio-temporal regression-kriging and multiple linear regression models.

Position (area in m^2)	Separable	Metric	Product-sum	Sum-metric	Long term observation
Inter-row position (8.20)	5.07	5.06	5.13	5.10	–
Fertilization point (3.60)	5.00	5.02	5.03	5.03	–
Under the tea tree (21.6)	7.46	7.44	7.34	7.44	–
In the tea tree row (3.60)	0.861	0.868	0.842	0.867	–
Total amount (40)	18.4	18.4	18.3	18.5	14.7

GMDD
doi:10.5194/gmd-2015-251

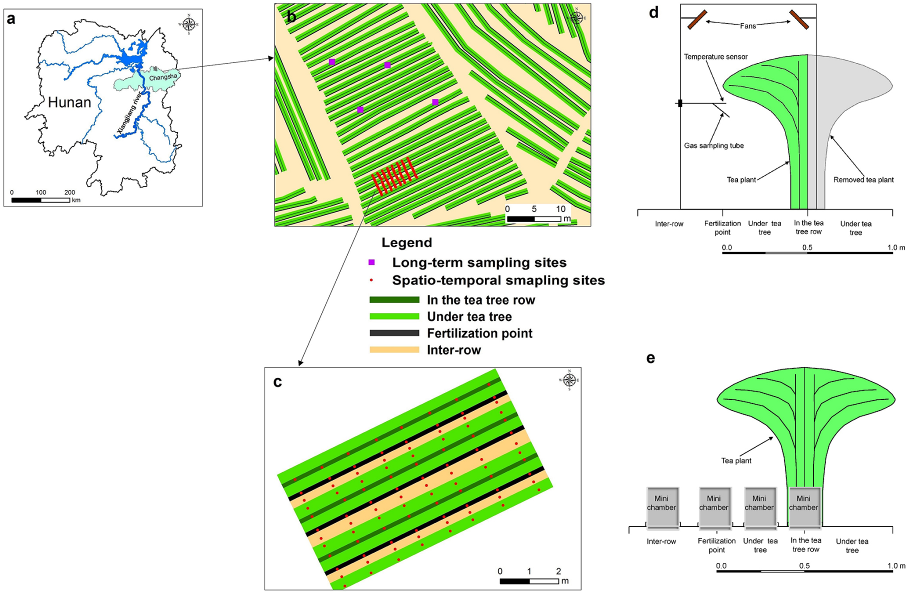

Figure 1. (a, b) Location and **(c)** land use map of the tea planted catchment, **(d)** a vertical transect of a tea tree row and a large static chamber and (e) the mini static chambers used to measure N_2O emissions from the tea field. The red circles in **(b, d)** represent the sampling points for researching the spatio-temporal structure of the N_2O fluxes, and the purple squares in **(d)** represent the sampling points for the long-term observation of the N_2O fluxes. The tea field is located in Jinjing Town, which is located 70 km northeast of Changsha, the capital city of Hunan Province, China.

GMDD
doi:10.5194/gmd-2015-251

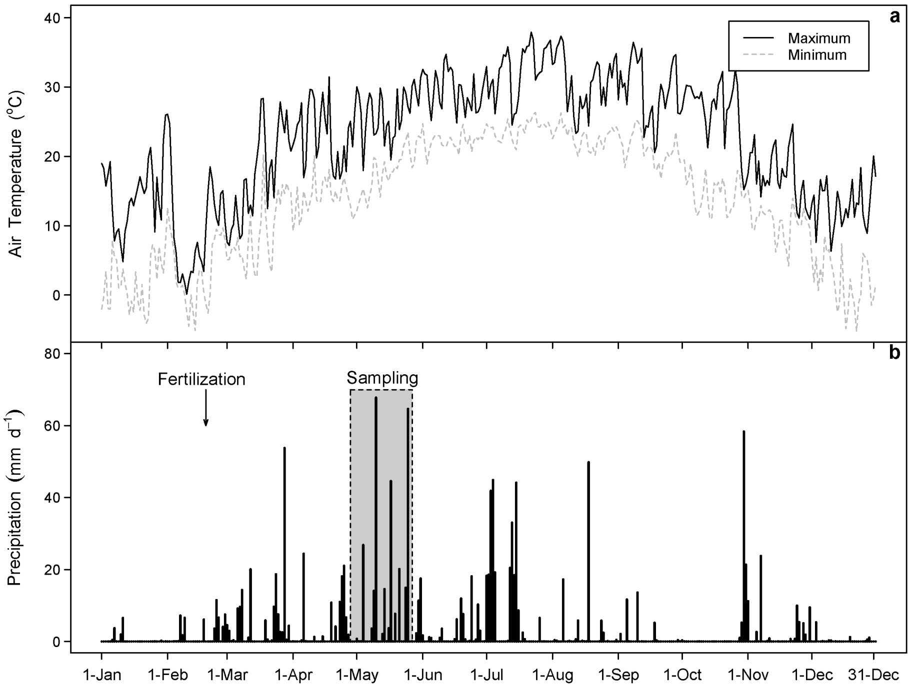

Figure 2. Daily **(a)** air temperatures and **(b)** precipitation during 2014.

GMDD
doi:10.5194/gmd-2015-251

Spatio-temporal variability in N_2O emissions

X. L. Liu et al.

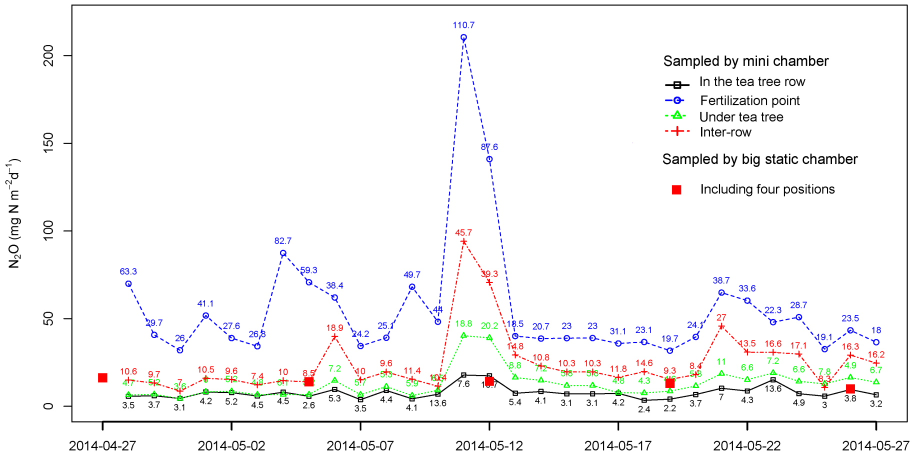

Figure 3. Dynamic temporal variations observed in the N_2O fluxes ($mg\,N\,m^{-2}\,d^{-1}$) at the four positions (inter-row position, fertilization point, under the tea tree, and in the tea tree row) using the mini static chambers and at the tea tree row transect using the large static chambers. The numbers near the points indicate the standard error on the mean ($n = 96$).

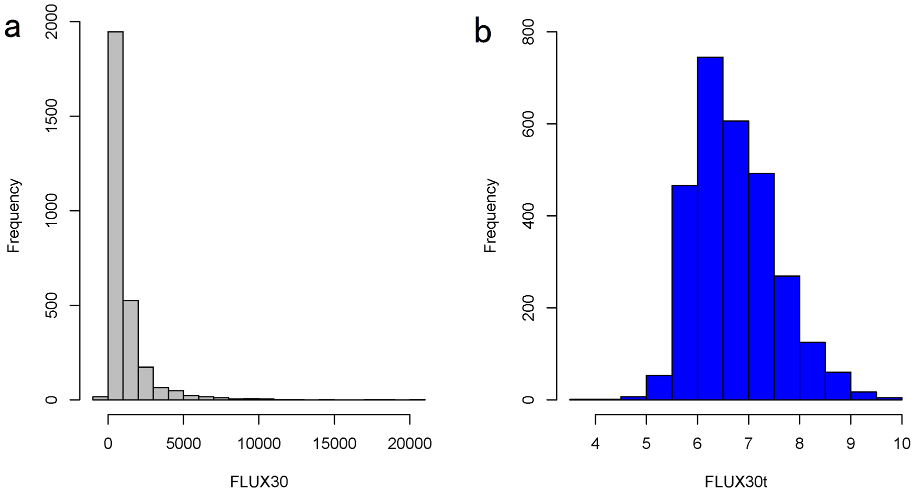

Figure 4. Histograms of **(a)** the original N_2O fluxes (FLUX30) and **(b)** the log-transformed N_2O fluxes (FLUX30t).

GMDD
doi:10.5194/gmd-2015-251

Spatio-temporal variability in N_2O emissions

X. L. Liu et al.

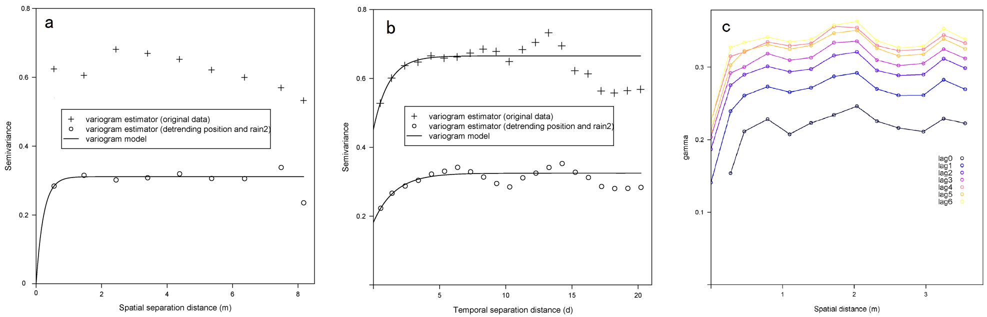

Figure 5. Semivariogram of the original data (pluses) and the residuals (open circles) of the N_2O fluxes from the multiple linear regression with the chamber placement positions (Position) and precipitation accumulated over two days (Rain2) as the predictors at the **(a)** spatial and **(b)** temporal scales. **(c)** The spatio-temporal semivariogram of the N_2O flux residuals.

GMDD
doi:10.5194/gmd-2015-251

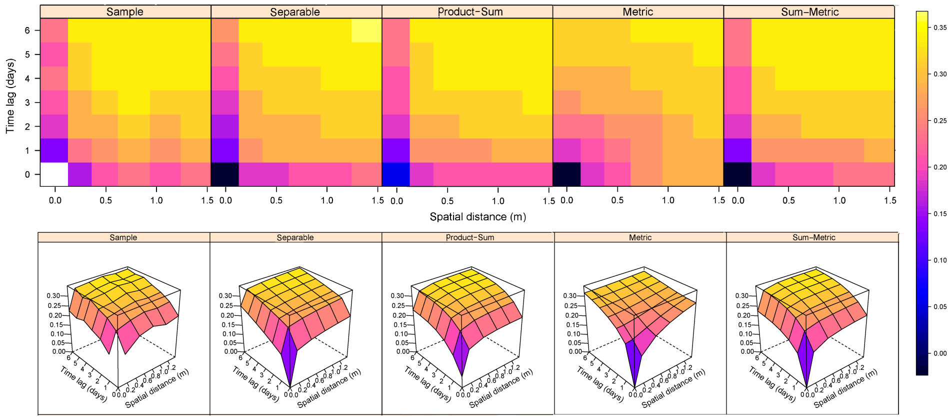

Figure 6. Sampled semivariogram and the fitted separable, product-sum, metric and sum-metric models of the N_2O flux residuals with Position and Rain2 as the predictors.

GMDD
doi:10.5194/gmd-2015-251

Title Page
Abstract Introduction
Conclusions References
Tables Figures
◄ ►
Back Close
Full Screen / Esc
Printer-friendly Version
Interactive Discussion

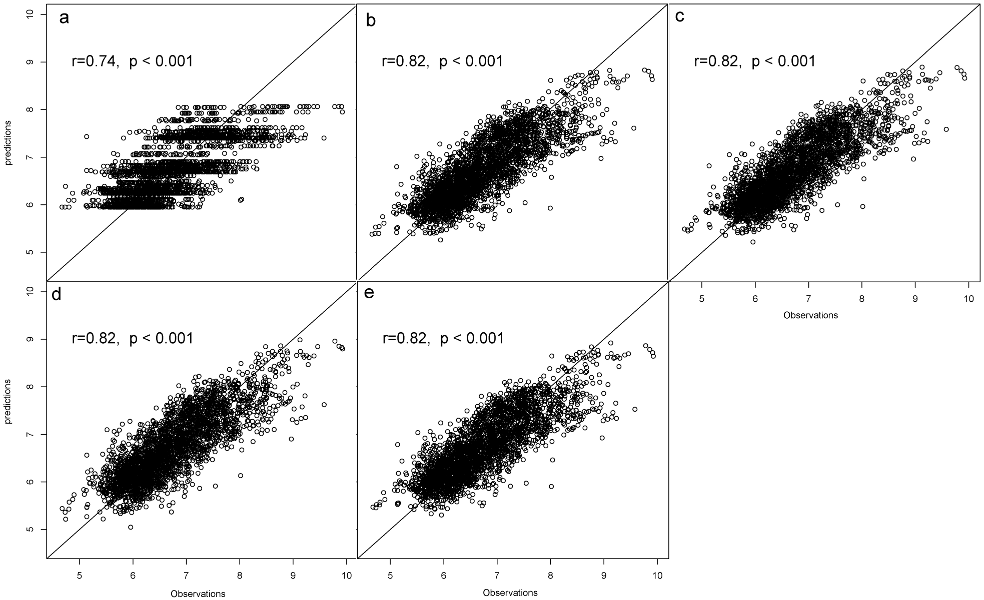

Figure 7. Cross-validation plots for **(a)** the multiple regression linear model and **(b–e)** the spatio-temporal regression-kriging models: **(b)** separable, **(c)** product-sum, **(d)** metric, and **(e)** sum-metric.

GMDD
doi:10.5194/gmd-2015-251

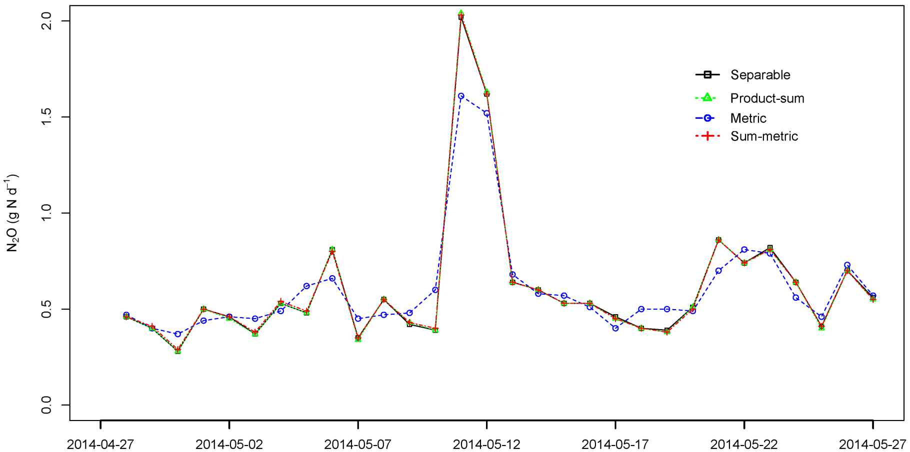

Figure 8. The temporal dynamics of the daily amounts of N_2O emissions ($g\,N\,d^{-1}$) obtained using the four models to fit the semivariograms in spatio-temporal regression-kriging.

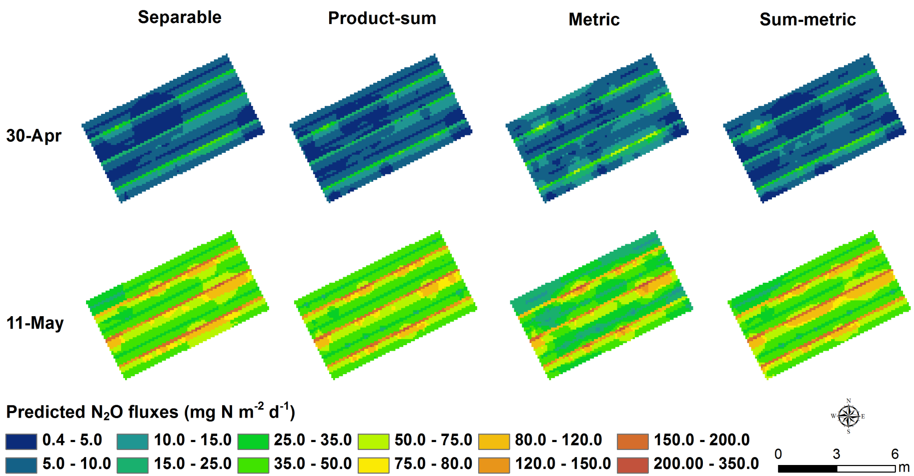

Figure 9. Spatio-temporal interpolations of the daily N_2O fluxes ($mg\,N\,m^{-2}\,d^{-1}$) on 30 April with the lowest daily amount of N_2O emissions and 11 May with the highest daily amount of N_2O emissions, obtained using the four models to fit the semivariograms in spatio-temporal regression-kriging.

GMDD
doi:10.5194/gmd-2015-251

Spatio-temporal variability in N_2O emissions

X. L. Liu et al.